Turbulence, Heat and Mass Transfer 7

A finite element LES methodology for anisotropic inhomogeneous meshes

Jonathan R. Bull, Matthew D. Piggott, Christopher C. Pain

Applied Modelling and Computation Group, Department of Earth Science and Engineering, Imperial College London, Prince Consort Road, London SW7 2BP, UK.

j.bull08@imperial.ac.uk

Abstract —

Large eddy simulation techniques offer a wealth of valuable information for engineering design purposes, but in many cases the required mesh resolution is prohibitive. Combining the dynamic LES procedure with unstructured mesh adaptivity offers a robust and efficient way of capturing the inhomogeneity and anisotropy of complex turbulent flows. However, this may result in a non-vanishing commutation error due to the filter employed. The inverse Helmholtz filter is used here with a tensor definition of filter width related to the local element size and shape. The formulation, verification and validation of a finite element methodology, designed to yield maximal accuracy from moderate mesh resolution with minimal *ad hoc* procedures, is described. Results for the 3D backward facing step obtained using the open source CFD code Fluidity are presented. Using adaptive meshing, closer agreement to DNS was obtained compared to fixed meshes while using 60% fewer nodes.

1. Introduction

As a complement to experiments and RANS simulations, LES has the potential to reduce industrial product development timescales, costs and uncertainties. State-of-the-art large eddy simulation techniques are starting to be applied beyond the idealised constructs of academia and onto problems of genuine industrial relevance [1]. For example, analysis of thermal fatigue, turbulent mixing and buoyancy-driven convection are all accessible through LES.

However, until recently there have been significant barriers to the widespread adoption of LES outside of academia. Conventional LES turbulence models may be non-robust to variations in geometry and meshing, and significant trial and error goes into finding the optimum model/mesh configuration for a given geometry. Uniformly fine meshes, and consequently, long simulation times are *de rigeur* but adequate computing resources are prohibitively expensive to many industry users.

An efficient use of computational resources is afforded by unstructured adaptive meshing, automatically refining the mesh only where and when it is needed according to local flow conditions [2]. The approach is ideal for complex geometries compared to a structured mesh which can be difficult and time-consuming to create, and the location of important flow features may not be known *a priori*. To make the most of the mesh refinement the LES filter width can be related to the local mesh size but this introduces commutation errors [3]. The inverse Helmholtz operator was proposed as an ideal filter for this purpose in [4].

If the LES filter width is placed at the far end of the inertial range of turbulence (by choice of mesh refinement), then the sub-filter-scale (SFS) motions are theoretically isotropic [5]. LES models commonly make this assumption, thus prescribing a fine mesh. The approach taken in this paper, motivated by practical limits on industrial computing resources, is to limit mesh resolution and consign a greater fraction of the turbulent kinetic energy to the SFS scales (similar to the VLES approach [6]). This can be done without the filter width approaching the integral scale and causing gross modelling errors, although in turbulent boundary layers some parame-

terisation such as wall functions is still required [1]. In simulations of flow across tube bundles, under-resolved LES was found by [7] to be sufficiently accurate for industrial purposes.

While the dynamic LES framework of [8] captures the spatial variations (inhomogeneity) of the SFS scales by means of a spatially-varying coefficient, few attempts have been made to properly account for mesh anisotropy in an LES model. The scale-similarity model [9] used a tensorial 'box' filter on anisotropic Cartesian meshes, and [10] proposed an anisotropy correction factor for Cartesian meshes, but the problem is more difficult on unstructured meshes. A tensorial filter width definition was proposed in [11] to form the basis of a tensor Smagorinsky model with unstructured meshes; good agreement was obtained in bluff body flows with coarse resolution. In this work the tensorial filter width is extended to the dynamic LES framework by incorporating it into the inverse Helmholtz filter operator, as suggested in [4].

In practical terms, an ideal CFD methodology is one that does not need to be tuned to a particular situation, optimises use of computational resources, captures the inherent inhomogeneity and anisotropy of turbulence and whose accuracy is well quantified. In this work, a tensorial eddy viscosity model is used in the dynamic procedure with a tensorial inverse Helmholtz filter and unstructured mesh adaptivity, which has an enhanced ability to represent anisotropic SFS motions, in an attempt to realise this ideal. Verification and validation have been performed using the finite element code Fluidity; more details on the code can be found in [12]. Results for the 3D backward-facing step are presented.

2. Model details

The filtered incompressible momentum equation is written

$$\overline{\mathbf{u}}_t + \nabla.(\overline{\mathbf{u}\mathbf{u}^\mathbf{T}}) - \frac{1}{Re} \triangle \overline{\mathbf{u}} + \nabla \overline{p} + \nabla.\tau = \overline{\vec{F}} + E_c, \tag{1}$$

where $\overline{\vec{F}}$ are body forces, $\overline{(\ldots)}$ denotes the application of a spatial filter and $\tau = \overline{\mathbf{u}\mathbf{u}^\mathbf{T}} - \overline{\mathbf{u}}\,\overline{\mathbf{u}}^T$ is the stress tensor. $E_c(\overline{\mathbf{u}}, \overline{\triangle})$ is the total commutation error, which has several components; the particular error considered here is $E_c = \overline{\nabla(\phi)} - \nabla(\overline{\phi})$.

The Smagorinsky model, based on the eddy viscosity hypothesis, is well known and often used for the deviatoric stress tensor:

$$\tau_{ij} - \frac{1}{3}\tau_{kk}\delta_{ij} = -\nu_T \left[\nabla\overline{\mathbf{u}} + (\nabla\overline{\mathbf{u}})^T\right] = -2C_S^2\overline{\triangle}^2 \left|\overline{S}\right| \left[\nabla\overline{\mathbf{u}} + (\nabla\overline{\mathbf{u}})^T\right], \tag{2}$$

where the constant is usually taken as $C_S \approx 0.1$ and $\left|\overline{S}\right|$ is the rate of strain modulus. A common definition of the filter width $\overline{\triangle}$ in 3D is the cube root of the element volume V [13]:

$$\overline{\triangle} = V^{1/3}. \tag{3}$$

Picking a suitable value of the constant is impossible because it is flow-dependent, except in the case of homogeneous, isotropic and stationary turbulence [3]. It is this that the dynamic procedure addresses.

2.1. Tensor eddy viscosity model

The tensor eddy viscosity SFS model developed by [11] is a variation of (2) that can be applied consistently to unstructured triangular or tetrahedral meshes with finite element discretisations. The LES filter width $\overline{\triangle}$ is redefined as a tensor $\overline{\triangle}^2_{ij}$ related to the anisotropy of the mesh, so

that the model diffusion is scaled independently in each spatial direction and at each point in the domain. This is particularly useful in combination with unstructured mesh adaptivity where the mesh is refined or coarsened according to the local flow conditions. The model is written

$$\boldsymbol{\nu}_{T,ij} = C_S^2 |\overline{S}| \overline{\triangle}_{ij}^2, \tag{4}$$

$$\overline{\triangle}_{ij}^2 = \alpha^2 \triangle_{ij}^2 = \alpha^2 \mathbf{V}^T \mathcal{M}^{-1} \mathbf{V} = \alpha^2 \mathbf{V}^T \begin{bmatrix} h_\zeta^2 & 0 & 0 \\ 0 & h_\eta^2 & 0 \\ 0 & 0 & h_\xi^2 \end{bmatrix} \mathbf{V}, \tag{5}$$

where $\boldsymbol{\nu}_T$ is a tensor eddy viscosity, C_S is the Smagorinsky coefficient, $\triangle_{ij}$ is the element size tensor, h_i are the size components in local (element) coordinates. $\mathcal{M}^{-1}$ is a metric tensor calculated as part of the mesh adaptivity algorithm in Fluidity (see [2]) and the transformation $\mathbf{V}^T ... \mathbf{V}$ is the rotation from local (element) to global (Cartesian) coordinates. The parameter α determines filter width; $\alpha = 2$ has been reported to provide a better resolution of the highest-frequency resolved scales [5]. Use of the tensor SFS model with the dynamic procedure is investigated.

2.2. Dynamic procedure

The concept of the dynamic LES procedure is to derive an SFS stress term from the finest resolved scales. These are elucidated by filtering the velocity field with two filtering operations sequentially [8]. The shortcoming of the Smagorinsky model is addressed by using this extra information to calculate a spatially varying coefficient. The idea actually predates the dynamic model: [9] described the difference between two filtered fields as a natural way to estimate the SFS scales by invoking the scale-similarity assumption and also introduced the idea of a tensorial eddy viscosity.

The first or 'mesh' filter $\overline{G}(\mathbf{u})$ is usually taken to be an unknown filtering operation implicit in the choice of discretisation and mesh, although it can be an explicit operation on the discrete field. The second or 'test' filter $\widetilde{G}(\overline{\mathbf{u}})$ is an explicit operation on the mesh-filtered field $\overline{\mathbf{u}}$, resulting in the twice-filtered field $\widetilde{\overline{\mathbf{u}}}$. Whilst the mesh filter may be prescribed, the shape, size and form of the test filter operator must be chosen. Using this notation, two SFS stress tensors are written

$$\begin{aligned} \tau_{ij} &= \overline{u_i u_j} - \overline{u}_i \overline{u}_j, \\ T_{ij} &= \widetilde{\overline{u_i u_j}} - \widetilde{\overline{u}}_i \widetilde{\overline{u}}_j, \end{aligned} \tag{6}$$

where the overbar and tilde are associated with the action of the first and second filter operations respectively. The intermediate turbulent stresses, known as the Leonard tensor, are defined by

$$\mathcal{L}_{ij} = T_{ij} - \widetilde{\tau}_{ij} = \widetilde{\overline{u}_i \overline{u}_j} - \widetilde{\overline{u}}_i \widetilde{\overline{u}}_j. \tag{7}$$

Any eddy-viscosity model may be used to model the stress tensors, but in the original form the Smagorinsky model (2) is used. Substituting (2) into (6) and contracting with the rate of strain $\overline{S}_{ij}$:

$$\mathcal{L}_{ij} \overline{S}_{ij} = -2C_S^2 (\widetilde{\overline{\triangle}}^2 |\widetilde{\overline{S}}| \widetilde{\overline{S}}_{ij} \overline{S}_{ij} - \overline{\triangle}^2 \widetilde{|\overline{S}| \overline{S}_{ij}} \overline{S}_{ij}), \tag{8}$$

from which the 'constant' C_S (now a variable) is derived following the method of [14]. Note that C_S can only removed from the filtering operation by assuming it is constant. This mathematical

inconsistency has been addressed by [15] and others, but at the expense of model programmability [16]. In simulations C_S became oscillatory and unbounded, and either averaging of (7) over homogeneous flow directions or *ad hoc* 'clipping' of the values of C_S was required [17]. Neither is desirable, since they imply non-robustness. In the present approach, the combination of a novel filter and tensor model will be tested to see if it obviates these *ad hoc* procedures.

In order to allow use of the same coefficient C_S in both SFS models (6), self-similarity is assumed in the scales of motion in which the first and second cutoff wavelengths lie. That is, both scales lie within the inertial range of the turbulent cascade [18]. Self-similarity depends on two conditions: firstly that the filters are self-similar (in turn requiring knowledge of the shape of the filters), and secondly that a sufficiently fine mesh is used so that most of the turbulent energy is resolved and only the dissipative (homogeneous isotropic) scales are modelled.

The first condition is met thanks to the finding of [19] which was as long as their widths were defined identically, the exact choice of filter did not affect the results of the dynamic LES procedure. Here, the tensorial definition is used for both filters. For practical reasons, it may not be possible to meet the second requirement, especially at high Reynolds number. It is proposed that by building a model with enhanced capability to represent anisotropy in the SFS scales, the mesh resolution requirement can be relaxed without a drastic loss of accuracy. Results from the 3D backward facing step show that this approach is successful.

2.3. Filtering

Two approaches to filtering are possible: either implicit filtering on the grid and test filtering with another filter [20], or explicit filtering using two (known) similar filter kernels [21]. In the research presented in this paper, both approaches have been tested using a differential filter operator.

In the first approach, the shape of the first filter is implicit in the discretisation and one identifies the filter width with the mesh size. The filter width may be scaled up from the mesh size to provide a better representation of the scales at the cut-off point, as recommended by [5]. The second filter is explicit. In the special case of a Cartesian grid with central differencing, the implicit numerical filter is identical to the box filter of width $2\triangle$ where $\triangle$ is the mesh size [20]. In this case, the box filter can be used as the second filter and the scale-similarity assumption is not violated. However, in the case of an unstructured mesh, the numerical filter is not known. Implicit filter kernels have been derived for the finite element method but the analysis is beyond the scope of this paper; see [19], [22].

In the second approach, both first and second filters are explicit operations with widths larger than the mesh: $\overline{\triangle} = \alpha\triangle$, $\widetilde{\triangle} = \beta\triangle$ and $\alpha, \beta \geq 1$. While this results in extra computational work, it avoids the difficulties of knowing the implicit filter in the discretisation. This latter method was used by [8] in turbulent channel flow and by [23] in dynamic LES of the atmospheric boundary layer with the sharp spectral cut-off filter at both levels.

The inverse Helmholtz filter, introduced by [4] in the context of LES, is defined by the differential equation

$$\mathbf{u} = \overline{\mathbf{u}} - \nabla . \left(\frac{\overline{\triangle}^2}{24} \nabla \overline{\mathbf{u}} \right) . \tag{9}$$

where $\mathbf{u}, \overline{\mathbf{u}}$ are the unfiltered and filtered fields. The factor 24 makes the second moment the same as that of the Gaussian filter [24]. It was recommended by [25] for use in complex 3D domains on account of its ability to be supplemented with boundary conditions and has been used by e.g. [24], [26] for a variety of subgrid models. Useful properties are that the correlation

between two functions, and the mean of a derivative, are expressible in terms of the resolved scale, and the commutation error converges to zero for constant filter width in the limit $\overline{\triangle} \to 0$ [27].

Here the filter is applied to unstructured anisotropic meshes, as suggested in [4], by relating the filter width to the mesh size: $\overline{\triangle}_{ij}^2 = \alpha^2 \triangle_{ij}^2$ as in (5). The commutation error is no longer zero, but is related to the gradient of the spatially varying filter width, so that a smoothly varying mesh size reduces the error [28]. It was also noted in [27] that the commutation error could be expressed in terms of the resolved variable, opening up interesting modelling possibilities. The strong Dirichlet condition $\overline{\mathbf{u}} = \mathbf{u}$ and a zero Neumann condition are applied on solid boundaries.

The scalar, or isotropic, filter width (3) has also been used in the inverse Helmholtz operator. It resulted in a less dissipative dynamic LES procedure than the tensor form (5), possibly because the tensor filter's volume (its 2-norm) is larger than the scalar filter volume on the same element. The tensor form is consequently normalised to give the same volume:

$$\overline{\triangle}^2 = \alpha^2 \left(\frac{V^{2/3}}{||\mathbf{V}^T \mathcal{M}^{-1} \mathbf{V}||_2} \right) \mathbf{V}^T \mathcal{M}^{-1} \mathbf{V}. \tag{10}$$

2.4. Tensor dynamic procedure

Tensor eddy viscosity models have been proposed before: for example the scale-similarity models of [9] and [29]. These models are similar to the dynamic procedure in that they form a stress tensor by repeated application of a filter to the resolved velocity. The current model is broadly similar to these but is simpler than the model of [9] and has a more sophisticated filter width definition.

The tensor eddy-viscosity model (4) is incorporated in the dynamic procedure. First (mesh) filtering is done implicitly by the mesh with an assumed width $\overline{\triangle}^2 = \alpha^2 \triangle^2$. The second (test) filtered velocity $\widetilde{\overline{\mathbf{u}}}$ is obtained by an explicit filter operation, namely the global solution of the discretised form of equation (9) with the combined filter width

$$\widetilde{\overline{\triangle}}^2 = \widetilde{\triangle}^2 + \overline{\triangle}^2 = (\alpha^2 + \beta^2) \triangle^2, \tag{11}$$

where β is a scale factor between the second filter and the mesh size. This is different to some implementations of the dynamic procedure, as described in [3], in which β is a scale factor between the second and first filters.

Explicit first filtering with the inverse Helmholtz filter was also implemented for comparison purposes. Although the scale-similarity assumption implies that the first and second filters must have similar shapes, it was found that implicit instead of explicit filtering made a negligible difference to the solution and saved computation time. The reason for this may be that the effect of the first filter is only on the information contained in the filtered scales, i.e. the strain rate and Leonard terms in (12), and not on the filter width definition itself.

Another reason may be that in discretised form the inverse Helmholtz filter is similar to the implicit filter, in which case the first requirement of self-similarity is met. Indeed, to second order accuracy several common filters are identical in discrete form. It is beyond the scope of this paper to address this issue; see e.g. [19] for a detailed analysis.

The dynamic model coefficient, in the least-squares form of [14] is modified to permit a tensor $\overline{\triangle}$:

$$C_S(\mathbf{x},t) = -\frac{1}{2}\frac{\mathcal{L}_{ij}M_{ij}}{M_{kl}^2} = -\frac{1}{2}\frac{\mathcal{L}_{ij}(|\widetilde{\overline{S}}|\widetilde{\overline{S}}_{ij}\circ\widetilde{\overline{\triangle}}_{ij}^2 - \widetilde{|\overline{S}|\overline{S}_{pq}}\circ\overline{\triangle}_{pq}^2)}{(|\widetilde{\overline{S}}|\widetilde{\overline{S}}_{kl}\circ\widetilde{\overline{\triangle}}_{kl}^2 - \widetilde{|\overline{S}|\overline{S}_{mn}}\overline{\triangle}_{mn}^2)^2}, \tag{12}$$

where $\circ$ indicates a pointwise product. This formulation is mathematically consistent as it preserves the stress-strain alignment of the Smagorinsky eddy viscosity model. With (4) this forms an SFS model capable of representing anisotropic inhomogeneous sub-filter scales on an unstructured mesh.

2.5. Boundary Conditions

It is well known that most LES models cause errors near the wall in turbulent boundary layers because the integral scale of the flow becomes very small [1]. Consequently mesh resolution requirements become impractical beyond moderate Reynolds numbers [30]. Wall functions should be used to ensure the correct behaviour but the dynamic procedure may not be grossly inaccurate without them. In the results presented here no wall functions are used in order to isolate the effect of the model. No-normal flow was imposed on the sides of the domain, strong no-slip on the bottom and step, and zero-pressure on the outflow. To generate realistic turbulent inflow conditions, the synthetic eddy method (SEM) of is used [31]. SEM is a statistical reconstruction of a turbulent flow based on prescribed mean, Reynolds stress and lengthscale profiles. For the backward facing step the data was obtained from the DNS data of [32].

3. Verification and validation

3.1. MMS Tests

The tensor dynamic model has been implemented in the general-purpose CFD code Fluidity. Numerical properties of the methodology have been verified by obtaining convergence of the modelling errors using the method of manufactured solutions (MMS) [33]. A Gaussian bump scalar field $\phi(x,y)$ was prescribed on a 2×2 square with zero advection. The meshes labelled A-E had $2^3 - 2^7$ nodes per side, doubling from one mesh to the next, yielding approximately quadruple the number of elements. The scalar and tensor inverse Helmholtz filters were used to filter the field. Convergence was measured in the L_2 norm over the entire domain. Tests used the $P1-P1$ continuous Galerkin finite element discretisation so a maximum of second-order convergence is expected.

Figures 1 (a) - (c) show the convergence rate of $|\phi-\overline{\phi}|$, the commutation error $E_c = |\overline{\nabla(\phi)} - \nabla(\overline{\phi})|$, and convergence rate of the commutation error for both filters and both structured and unstructured tetrahedral meshes. On structured meshes the filtered field convergence rate tends to second order and the commutation error also converges at close to second order. On unstructured meshes the convergence rate is lower but tends towards second order as the mesh is refined. The commutation error convergence rate is much lower but still positive. The errors are sensitive to the meshing algorithm employed (advancing front was used here).

Figure (b) shows that the isotropic filter commutation error is consistently smaller than its anisotropic counterpart. The anisotropic filter width definition results in almost identical behaviour to the classic isotropic filter width definition, albeit with a slight increase in the commutation error. However, the use of either filter on unstructured meshes presupposes careful consideration of mesh design to improve smoothness.

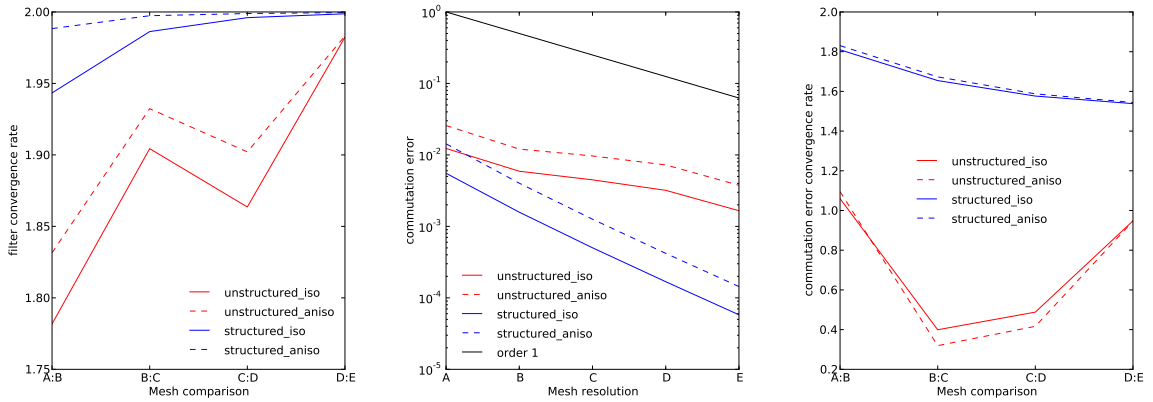

(a) Convergence rate of $|\phi - \overline{\phi}|$ (b) Commutation error E_C (c) E_C convergence rate

Figure 1: MMS test results

3.2. Backward facing step

Validation has been carried out using the 3D backward-facing step at $Re = 5100$, which is a valuable proving-ground for turbulence models for several reasons. Most importantly, there exists high-quality benchmark data from the DNS study of [34]. Secondly, the length of the separated eddy behind the step is a sensitive model performance indicator. Thirdly, the turbulence generated by the step is inhomogeneous and anisotropic. The influence of the filter shape, filter size ratios, limiting C_S and using an implicit or explicit first filter on several diagnostics are investigated.

Results using fixed and adaptive meshes are presented. The fixed mesh has an approximately uniform edge length of 0.125 and 596,000 nodes. The adaptive meshes vary from one simulation to another but the maximum number of nodes was approximately 235,000 and the edge lengths were approximately constrained to the range 0.05-1.0. Figure 2a shows an instance of an adaptive mesh with edge lengths 0.01-1.0. The adaptivity algorithm in Fluidity adjusts the mesh resolution locally to meet an interpolation error requirement on the velocity field (see [2] for further details).

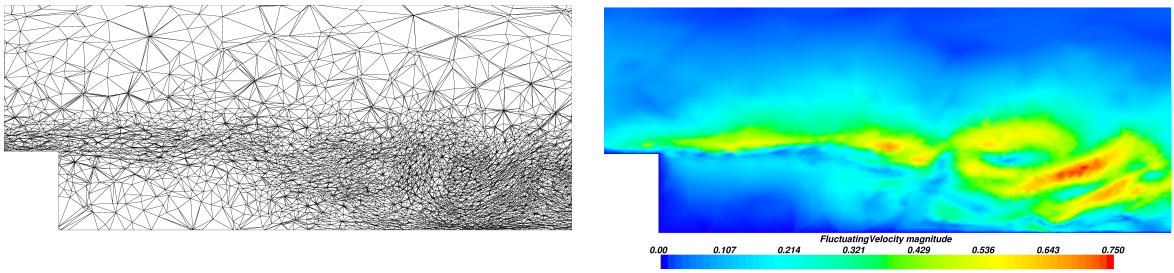

(a) Instance of adaptive mesh (b) Fluctuating velocity on adaptive mesh

Figure 2: Mesh adapting to fluctuating velocity field

Turbulent inflow conditions were provided by the synthetic eddy method (SEM) [31] which interpolated the data of [34]. A strong no-slip condition was applied on the bottom, and a region of absorption was defined near the outflow to reduce the chance of turbulent flow re-entering the domain and causing the solver to blow up. On adaptive meshes no-normal-flow conditions were

specified on the sides while the fixed mesh had periodic boundary conditions in the spanwise direction. Discretisation was by the continuous Galerkin finite element method with piecewise linear function spaces for velocity and pressure (p1p1-CG).

Simulations were run on the CX1 cluster at Imperial College London using 16-32 processors and 150 hours of run-time (≈ 500 seconds of simulated time). Predictions of reattachment length, mean and Reynolds stress profiles were compared to DNS data of [34] and dynamic LES data of [35] (which used a stretched Cartesian mesh of $148 \times 72 \times 20$ (213,120) nodes with finite volume discretisation and the dynamic model of [14] in which C_S was stabilised by averaging and clipping $C_S \geq 0$).

Table 1 lists the reattachment length (R_L) predictions. R_L was calculated by finding the point at which the velocity changed direction along several parallel lines close to the bottom, and taking the average value. Even after spanwise averaging the instantaneous reattachment point fluctuated greatly, and the results below are time averages. The adaptive results are better than those from the fixed periodic mesh indicating that a fine near-wall mesh is important to resolve the dynamics there. However, no-normal-flow side boundary conditions (used on adaptive meshes) have been found to exert a slight drag compared to periodic conditions (used on the fixed mesh). The effect on the results presented has not been fully quantified. Implementation of periodic boundary conditions with parallel mesh adaptivity is under way in Fluidity and will improve modeling capabilities. In terms of model parameters, the closest predictions are from models with $\alpha = 1$ and explicit filtering makes little difference.

model	mesh	R_L
DNS [34]	9.4M nodes	6.28
isotropic [35]	213k nodes	7.3
anisotropic Smagorinsky	fixed periodic	7.94
isotropic	fixed periodic	7.94
anisotropic	fixed periodic	7.77
isotropic	adaptive	7.74
isotropic $\alpha = 1$	adaptive	6.65
isotropic $\alpha, \beta = 1$	**adaptive**	**6.51**
anisotropic	adaptive	7.90
anisotropic $\alpha = 1$	**adaptive**	**6.68**
anisotropic $\alpha, \beta = 1$	adaptive	7.04
explicit isotropic	adaptive	7.52
explicit isotropic $\alpha = 1$	**adaptive**	**6.58**
explicit anisotropic	adaptive	8.20
explicit anisotropic $\alpha = 1$	**adaptive**	**6.75**
isotropic unlimited C_S	adaptive	7.27
isotropic $\alpha = 1$ **unlimited** C_S	**adaptive**	**6.55**
anisotropic unlimited C_S	adaptive	12.93
anisotropic $\alpha = 1$ unlimited C_S	adaptive	9.05

Table 1: Time averaged reattachment length in step heights. Anisotropic Smagorinsky refers to second order model (4). All other models are dynamic LES. **Bold** indicates top five results.

Figure 3 shows the mean velocity profiles obtained with adaptive meshing and isotropic filter, and Figure 4 the anisotropic filter results. All results used an implicit first filter. There is little difference between the isotropic and anisotropic models, although the anisotropic model is slightly more dissipative. Setting $\alpha = 1$ greatly improves the predictions of both the isotropic and anisotropic models, suggesting that the filter width is more important than the filter shape

in determining model dissipation. One reason for the observed insensitivity to the filter shape could be that although the mesh is adaptive, the elements in it are still fairly isotropic.

Figures 3 and 4 also show results in which the upper limit on C_S has been removed. This makes no difference compared to the equivalent limited isotropic case, but in the anisotropic case it makes the model more dissipative: removing the limit only makes C_S grow larger. These results imply that the isotropic model is more robust as it does not require limiting of the coefficient to make it stable. The anisotropic model is inclined to make the coefficient, and therefore the eddy viscosity, too large so the definition of the filter width may need to be revised. Figure 4 also shows results from the fixed mesh with the anisotropic filter and $\alpha = \beta = 2$. The profile is comparable to the equivalent adaptive run, indicating that the poorer R_L predictions on the fixed mesh are probably due to insufficient wall resolution, and that adaptive meshing with far fewer elements can capture the flow profile.

Other results using an explicit first filter showed no difference compared to using the filter implicit in the discretisation. This suggests that the procedure is insensitive to the filter shape, which is consistent with the above results, and also with the findings of [19] provided that the filter definition is used 'consistently' throughout the implementation. It is also possible that the implicit filter is similar to the inverse Helmholtz filter, at least to the second order accuracy of the p1p1-CG discretisation.

Figures 5a and 5b show the Reynolds stresses from the runs in Figures 3 and 4. Profiles were taken from the centre of the domain at a distance $x/h = 4$ behind the step where h is the step height. All are comparable to the results from [35] but the best are with no turbulence model and with $\alpha = \beta = 1$. The plots show some lack of smoothness which is due to the relatively short time averaging period of around $7 - 10$ flow-through periods (N.B. averaging was begun after reaching statistical steady state). The gradients near the wall are poorly represented and would benefit from reducing the minimum mesh size in the adaptivity algorithm.

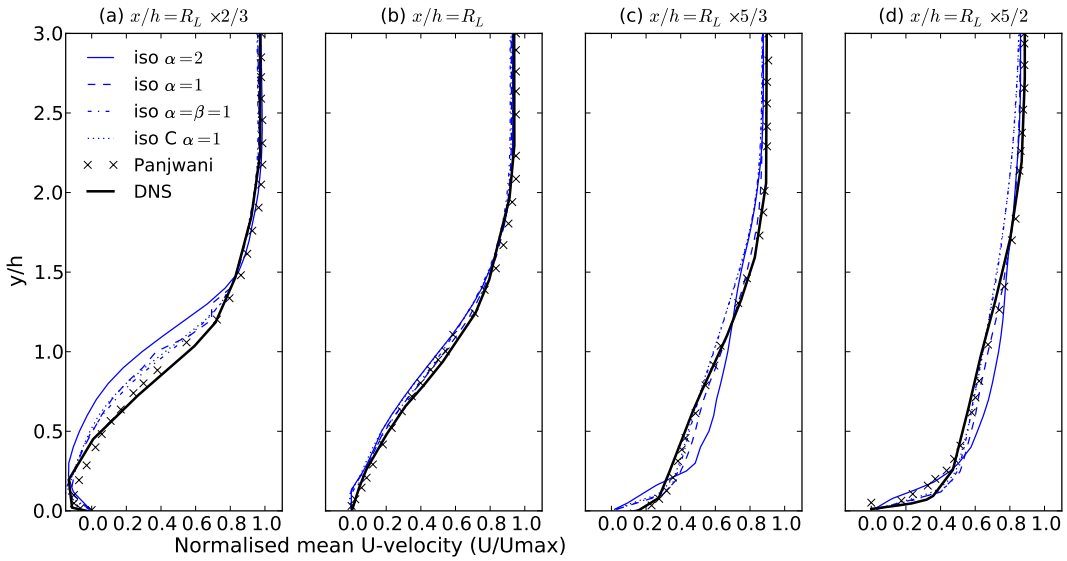

Figure 3: Mean velocity profiles, isotropic filter, adaptive mesh. 'DNS' = DNS of [34]; 'iso'/'aniso'= isotropic/anisotropic dynamic model, 'C' = no upper limit on C_S, 'F' = fixed mesh. $\beta = 1$ unless otherwise stated.

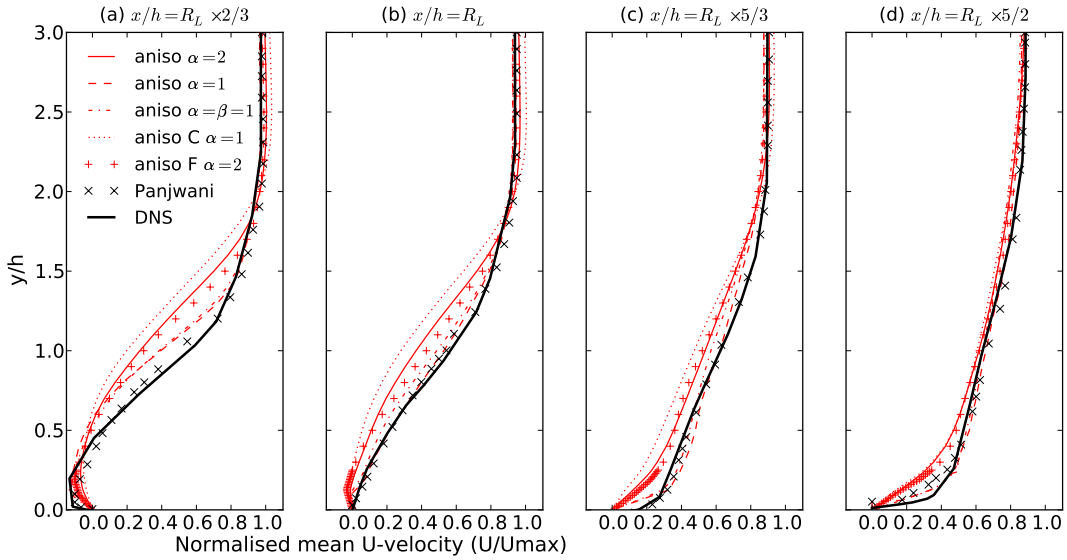

Figure 4: Mean velocity profiles, anisotropic filter, adaptive mesh. Key same as Figure 3.

4. Conclusions

A novel tensor dynamic LES procedure has been implemented and tested in the 3D backward facing step. Reattachment length predictions using the isotropic filter on adaptive meshes come within 4% of benchmark DNS data, and using the anisotropic filter within 7%. The combination of dynamic LES with unstructured mesh adaptivity improved upon the fixed-mesh results while using 60% fewer nodes, although this is partly because of superior near-wall resolution. The main positive effect on model accuracy is from setting the filter width parameter $\alpha = 1$, whereas the shape - scalar vs. tensor - made less difference.

Using an explicit first filter to satisfy the first condition of scale-similarity - the first and second filters having similar shapes - did not significantly affect the results, confirming the finding of [19] that ensuring the mesh and test filters are similar is not necessary. Removal of the upper limit on the Smagorinsky coefficient did not change the outcome when using the scalar filter indicating that the model is robust. The anisotropic filter's over-dissipative nature was enhanced when the limit was removed.

Work is continuing in an attempt to realise a robust parameter-free LES model which has great potential for reducing computational effort for complex industrial problems. For example, it may be possible to remove the *ad hoc* stability constraint $C_S \geq 0$. It also remains to be seen whether the anisotropic filter definition is superior on highly stretched meshes where a single value filter width cannot be fitted satisfactorily to high-aspect-ratio elements. More rigorous accuracy and reliability tests are also required.

References

[1] N. J. Georgiadis, D. P. Rizzetta, and C. Fureby. Large-eddy simulation: Current capabilities, recommended practices, and future research. In *47th AIAA Aerospace Sciences Meeting*, 2009.

[2] CC Pain, AP Umpleby, CRE De Oliveira, and AJH Goddard. Tetrahedral mesh optimisation and adaptivity for steady-state and transient finite element calculations. *Comp. Methods in Appl. Mech. and Eng.*, 190(29-30):3771–3796, 2001.

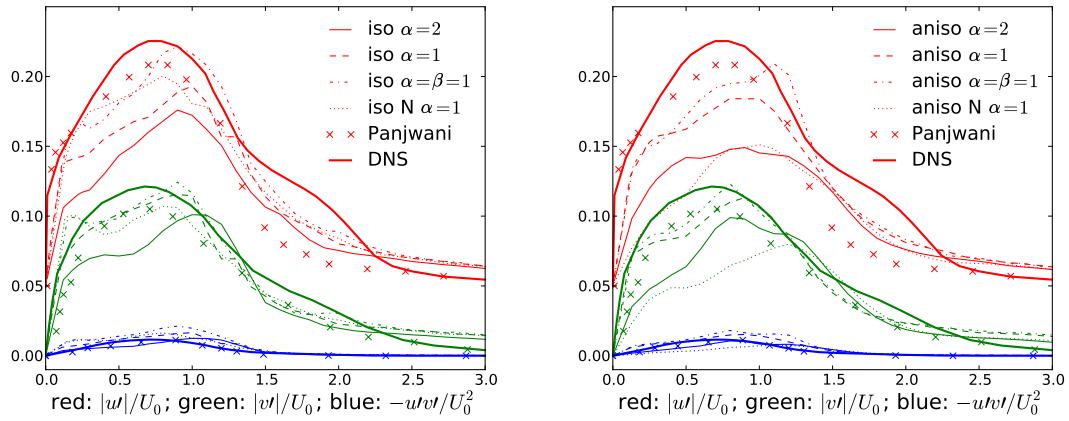

(a) Isotropic model (b) Anisotropic model

Figure 5: Reynolds stresses. Red lines shifted by 0.05. $C_S \leq 0.2$, $\beta = 2$ unless otherwise stated.

[3] P. Sagaut and C. Méneveau. *Large eddy simulation for incompressible flows: an introduction*. Springer Verlag, 2006.

[4] M. Germano. Differential filters for the large eddy numerical simulation of turbulent flows. *Phys. Fluids*, 29(6):1755–1756, 1986.

[5] S. B. Pope. *Turbulent Flows*. Cambridge Univ Press, 2000.

[6] J. Frohlich and D. von Terzi. Hybrid LES/RANS methods for the simulation of turbulent flows. *Progress in Aerospace Sciences*, 44:349–377, 2008.

[7] S. Benhamadouche and D. Laurence. LES, coarse LES, and transient RANS comparisons on the flow across a tube bundle. *Int. J. of Heat and Fluid Flow*, 24:470–479, 2003.

[8] M. Germano, U. Piomelli, P. Moin, and W. H. Cabot. A dynamic subgrid-scale eddy viscosity model. *Phys. Fluids*, 3(7):1760–1765, 1991.

[9] J. Bardina, J.H. Ferziger, and W.C. Reynolds. Improved subgrid-scale models for large-eddy simulation. In *AIAA 13th Fluid and Plasma Dynamics Conference*, July 1980.

[10] A. Scotti, C. Meneveau, and D. K. Lilly. Generalized Smagorinsky model for anisotropic grids. *Phys. Fluids*, 5(9):2306–2308, 1993.

[11] T. Bentham. *Microscale Modelling of Air Flow and Pollutant Dispersion in the Urban Environment*. PhD thesis, Imperial College London, 2003.

[12] Piggott MD, Gorman GJ, Pain CC, Allison PA, Candy AS, Martin BT, and Wells MR. A new computational framework for multi-scale ocean modelling based on adapting unstructured meshes. *Int. J. Num. Methods Fluids*, 56:1003–1015, 2008.

[13] J.W. Deardorff. A numerical study of three-dimensional turbulent channel flow at large reynolds numbers. *J. Fluid Mech*, 41(2):453–480, 1970.

[14] D. K. Lilly. A proposed modification of the Germano subgrid-scale closure method. *Phys. Fluids*, 4(3):633–635, March 1992.

[15] Sandip Ghosal, Thomas S. Lund, and Parviz Moin. A dynamic localization model for large-eddy simulation of turbulent flows. *J. Fluid Mech.*, 286:229–255, 1995.

[16] P. Sagaut. *Multiscale and multiresolution approaches in turbulence*. Imperial College Press, 2006.

[17] D. Carati, G. S. Winckelmans, and H. Jeanmart. On the modelling of the subgrid-scale and filtered-scale stress tensors in large-eddy simulation. *J. Fluid Mech.*, 441:119–138, 2001.

[18] D. Carati and E. van den Eijnden. On the self-similarity assumption in dynamic models for large eddy simulations. *Phys. Fluids*, 9(2165), 1997.

[19] A. E. Tejada-Martinez and K. E. Jansen. Spatial test filters for dynamic model large-eddy simulation with finite elements. *Comm. Num. Methods in Eng.*, 19:205–213, 2003.

[20] A. E. Tejada-Martinez and K. E. Jansen. A dynamic Smagorinsky model with dynamic determination of the filter width ratio. *Phys. Fluids*, 16(7), 2004.

[21] G. S. Winckelmans, A. A. Wray, O. V. Vasilyev, and H. Jeanmart. Explicit-filtering large-eddy simulation using the tensor-diffusivity model supplemented by a dynamic Smagorinsky term. *Phys. Fluids*, 13(5):1385–1404, 2001.

[22] S. B. Pope. Large-eddy simulation using projection onto local basis functions. In J. L. Lumley, editor, *Lecture Notes in Physics*, volume 566, pages 239–265. Springer, 2001.

[23] Fernando Porte-Agel. Dynamic subgrid-scale models for momentum and scalar fluxes in large-eddy simulations of neutrally stratified atmospheric boundary layers over heterogeneous terrain. *Water Resources Research*, 42, 2006.

[24] B. J. Geurts and D. D. Holm. Alpha-modelling strategy for LES of turbulent mixing. *Turbulent Flow Computation*, 66:237–278, 2004.

[25] J. Mullen and P. F. Fischer. Filtering technique for complex geometry flows. *Comm. Num. Methods in Eng.*, 15(1):9–18, January 1999.

[26] B. Vreman, B. Geurts, and H. Kuerten. Large-eddy simulation of the temporal mixing layer using the Clark model. *Theor. and Comp. Fluid Dyn.*, 8:309–324, 1996. 10.1007/BF00639698.

[27] M. Germano. Differential filters of elliptic type. *Phys. Fluids*, 29(6):1757–1758, 1986.

[28] S. Camarri, M. V. Salvetti, B. Koobus, and A. Dervieux. Large-eddy simulation of a bluff-body flow on unstructured grids. *Int. J. Num. Meth. Fl.*, 40(11):1431–1460, 2002.

[29] S. Liu, J. Katz, and C. Meneveau. On the properties of similarity subgrid-scale models as deduced from measurements in a turbulent jet. *J. Fluid Mech*, 275:83–119, 1994.

[30] Y. Zhou, J. G. Brasseur, and A. Juneja. A resolvable subfilter-scale model specific to large-eddy simulation of under-resolved turbulence. *Phys. Fluids*, 12(9):2602–2610, 2001.

[31] D. Pavlidis, G.J. Gorman, J.L.M.A. Gomes, C.C. Pain, and H. ApSimon. Synthetic eddy method for urban atmospheric flow modelling. *Boundary Layer Meteorology*, 2009.

[32] H. Le and P. Moin. Direct numerical simulation of turbulent flow over a backward-facing step. In *Annual Research Briefs*, 1992.

[33] P. J. Roache. Code verification by the method of manufactured solutions. *J. Fluids Eng.*, 124(1):4–10, 2002.

[34] H. Le, P. Moin, and J. Kim. Direct numerical simulation of turbulent flow over a backward-facing step. *J. Fluid Mech.*, 330:349–374, 1997.

[35] B. Panjwani, I. S. Ertesvag, A. Gruber, and K. E. Rian. Large eddy simulation of backward facing step flow. In *5th National Conference on Computational Mech.*, 2009.